Impact of fiber geometry, temperature, loading rate, and concrete mix on the pull-out resistance of iron-based shape memory alloy (Fe-SMA): Experimental investigation

Alireza Tabrizikahou[a,*], Mieczysław Kuczma[a], Moslem Shahverdi[b,c]

[a]*Institute of Building Engineering, Poznań University of Technology, Piotrowo 5, 60-965, Poznań, Poland*
[b]*Empa, Swiss Federal Laboratories for Materials Science and Technology, Dübendorf 8600, Switzerland*
[c]*School of Civil Engineering, University of Tehran, Tehran 4563-11155, Iran*

Abstract

Iron-based shape memory alloys (Fe-SMAs) exhibit unique shape-recovery behavior upon thermal heating, which makes them beneficial for a wide range of structural applications such as pre-stressing. One feasible application is the introduction of short Fe-SMA fibers into a concrete structure, which allows pre-stressing forces to be distributed uniformly and locally throughout the concrete matrix. However, to achieve optimal pull-out resistance and effectively transfer pre-stressing forces to the concrete matrix, a detailed understanding of their bond behavior with concrete under different circumstances is essential. To address this critical aspect, the current work describes an extensive experimental campaign to determine the pull-out resistance of Fe-SMA fibers embedded in high-performance fiber-reinforced concrete (HPFRC). The experiment included 72 specimens with varying temperature ranges for thermal heating, loading rate, fiber end shape, and concrete mixtures. The results showed that fibers having an end-hooked form had double the pull-out resistance as straight fibers. Furthermore, increasing the temperature was shown to dramatically decrease the pull-out resistance of end-hooked fibers while having minimal impact on the pull-out resistance of straight fibers. Moreover, concrete mixes with higher compressive and flexural strengths exhibited increased pull-out resistance. Lastly, the effect of the loading rate was found to be minimal, since increasing the loading rate by ten resulted in only a slight increase in

*Corresponding author
Email address: alireza.tabrizikahou@put.poznan.pl (Alireza Tabrizikahou)

pull-out resistance.

Keywords: Iron-based shape memory alloy (Fe-SMA), high-performance fiber-reinforced concrete (HPFRC), pull-out resistance, bond behavior, effect of temperature, effect of fiber geometry

1. Introduction

High-performance fiber-reinforced concrete (HPFRC) is a composite construction material made of concrete and randomly distributed short fibers of various materials [1, 2]. This type of concrete, known for its high compressive strength, improved tensile strength, and significant ductility due to fiber bridging [3, 4], is becoming increasingly popular in civil engineering applications for its superior properties [5, 6].

Shape memory alloys (SMAs) are unique metallic materials known for their ability to recover their original shape from seemingly permanent deformations when heated above some temperature A_f (austenite finish temperature) [7, 8]. This feature known as the shape memory effect (SME) is caused by a reversible martensitic phase transformation [9, 10]. SMAs have distinct features and considerable advantages over conventional metals such as steel, aluminum, and copper, making them suitable for a variety of industries, including aerospace, biomedical, automotive, and robotics [11, 12, 13, 14]. In recent years, interest in SMAs has grown in civil engineering, notably for applications like earthquake resistance and structural retrofitting [15, 16]. SMAs can improve the performance and resilience of civil structures by providing advantages such as pre-stressing, energy dissipation, self-centering, and self-healing [17, 18, 19]. Iron-based SMAs (Fe-SMAs), such as Fe-Mn-Si, stand out from other types of SMA due to their high recovery stress and reduced cost when compared to nickel-titanium (Ni-Ti) SMAs, making them suitable for civil engineering applications [20, 21, 22, 23].

Incorporating short Fe-SMA fibers into HPFRC introduces innovative and beneficial capabilities to the material [24, 25]. When pre-strained short Fe-SMA fibers are embedded into concrete, they are passive until heated [26, 27, 28]. Due to the SME feature, these fibers can pre-stress concrete due to the martensitic phase transformation upon thermal heating. For optimal performance, thermal heating should occur after

the concrete has hardened, ensuring the fibers are well anchored. When heated, the fibers attempt to return to their initial shape, resulting in pre-stressing forces that enhance the stiffness of the concrete. As a result, the interaction and bonding between short Fe-SMA fibers and the concrete matrix have a major impact on their pre-stressing efficiency and capacity to withstand external mechanical loads [29, 30].

To show the significance of obtaining the maximum pull-out resistance in such applications, Figure 1 illustrates an image from a pilot experiment in which concrete samples with short Fe-SMA fibers with end-hooked forms were subjected to the 3-point bending test. The enlarged picture of the fracture shows that fibers failed mainly due to pull-out, with straightened ends or no deformation in the end-hooked geometry. A detailed visual examination of the samples reveals that tensile failure of the fibers is a rare phenomenon. Instead, the most common failure mechanism is a loss of pull-out resistance between the fibers and the concrete matrix, or a lack of enough strength in the concrete matrix. Figure 2 illustrates the conceptual difference between the pull-out and tensile failure of fibers in cracked concrete. Figure 2a shows that when fibers lose their pull-out resistance and slip inside the concrete matrix, their tensile strength does not contribute to preventing crack growth. This leads to rapid crack growth and the probable collapse of the concrete structure. Figure 2b, on the other hand, shows that when fibers have sufficient pull-out resistance, they may withstand applied stresses, preventing crack formation inside the concrete until the fibers rupture in tension at their ultimate plastic strain. Ideally, obtaining maximum pull-out resistance is of great importance because it allows the fibers to significantly contribute to the structural integrity of the concrete. This guarantees that the failure process is dominated by tension fiber rupture rather than the rapid degradation observed in brittle materials such as concrete.

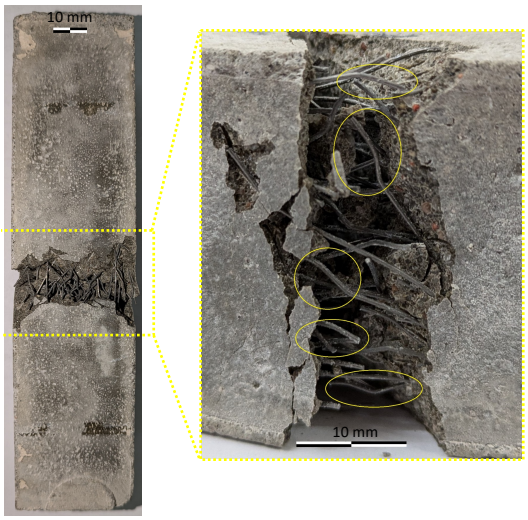

Figure 1: Bottom view of a concrete element with end-hooked short Fe-SMA fibers subjected to 3-point bending.

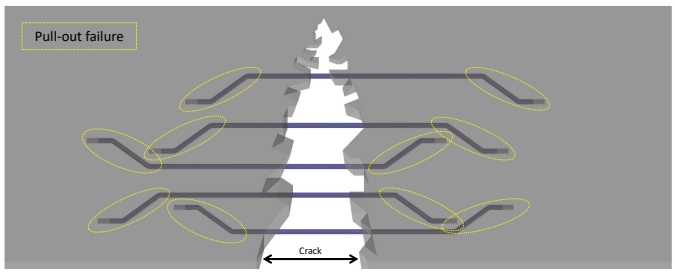

(a)

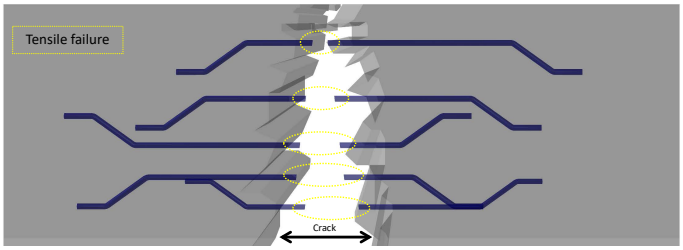

(b)

Figure 2: Schematic failure mechanisms in a fiber-reinforced concrete element with (a) pull-out, and (b) tensile failure.

In addition to experimental research, early computational modeling of concrete composites reinforced with Fe-SMA fibers has demonstrated the need to precisely define the contact constraints at the Fe-SMA fiber-concrete matrix interface to obtain reliable and accurate results. Other research has highlighted the significance of this feature [31, 32, 33, 34, 35, 36, 37, 38].

Several recent studies have focused on measuring and enhancing the fiber pull-out behavior in HPFRC composites. Dehghani et al. [39, 40] studied the pull-out behaviors of Ni-Ti SMA fibers (0.8 mm in diameter) embedded in self-compacting concrete and compared their behavior to steel fibers (0.75 mm in diameter). In their investigation, SMA fibers with a 45-degree curled end had the highest bonding strength of all the SMA fibers tested. Increasing the embedding length of both SMA and steel fibers significantly increased the pull-out force while maintaining the structure of the pull-out load-slip curve. SMA fibers were almost insensitive to loading rate during pull-out, yet steel fibers were significantly sensitive. The steel fiber interface exhibited considerable matrix deterioration, which may explain their rate sensitivity during pull-out due to the mechanical behavior of the concrete mixture. SMA fibers, on the other hand, showed no matrix degradation during pull-out, suggesting why the loading rate had little effect on their performance. Menna et al. [41] studied the pull-out behavior of cold-treated Ni-Ti SMA fibers in three different types of concrete mixes, taking into account thermal processing and end-hook shape (3D, 4D, 5D). Thermal processing at 350°C for 20-40 minutes yielded the finest results. SMA fiber topologies with 5D in normal strength concrete, 4D and 5D in high-performance concrete, and 3D and 4D in ultra-high-performance concrete outperformed steel equivalents in terms of cyclic loading and re-centering.

Yang et al. [42] investigated the cyclic pull-out behavior of Ni-Ti SMA fibers embedded in an ECC mixture, using three types of fiber ends: straight, hooked, and knotted. They found that fibers ending with knots had sufficient adhesive strength, with a peak pull-out force of around 1100 MPa, triggering their superelastic properties. These fibers showed great self-centering capabilities, with low residual displacement (0.29 mm) and a maximum self-centering ratio of 93%. Increasing the bonding length of SMA fibers with knotted ends resulted in higher ultimate strain but lower maximum

pull-out force. Furthermore, the ultimate strain and stress of knotted-end SMA fibers increased with increasing fiber thickness. Surprisingly, the researchers discovered that differences in bonding length and fiber thickness had no effect on the self-centering ratio. Wang et al. [43] found that SMA-FRC failed predominantly through pull-out, with no apparent Ni-Ti fiber deformation. This phenomenon was related to the superelastic characteristics of cold-drawn NiTi-SMA fibers. Other samples, on the other hand, showed a failure mechanism dominated by pull-out with some fiber fracturing. The principal cause of failure in these non-SMA specimens was the concrete mix's low loading ratio and modest crack width, which resulted in reduced fiber fracture.

While all the aforementioned studies measured the pull-out behavior of Ni-Ti SMA fibers, to the author's best knowledge, there is no available research on the pull-out behavior of Fe-SMA short fibers in concrete, including the impact of thermal heating, concrete mix design, loading rate, and fiber shape. This study attempts to fill this gap by experimentally investigating these aspects. In the current study, 24 groups of specimens, each with three samples (a total of 72 specimens), were tested to measure the pull-out resistance of Fe-SMA fibers in a concrete matrix. In addition, various samples were tested to determine the concrete's mechanical properties. Since the use of Fe-SMA short fibers in concrete structures for pre-stressing applications involves a variety of thermomechanical processes such as thermal heating and mechanical loadings, this study investigated the impact of thermal heating and high temperatures on the mechanical properties of the concrete and the pull-out resistance of Fe-SMA fibers embedded within the concrete matrix. The temperature ranges of ambient (without thermal heating), 160°C, and 200°C were evaluated. Furthermore, two different fiber end geometries, straight and end-hooked, were tested in order to determine how they impacted the pull-out resistance of Fe-SMA fibers. Two distinct concrete mix designs were tested to investigate how concrete density, compressive strength, and flexural strength influenced Fe-SMA fiber pull-out resistance. Finally, two different loading rates were assumed to study whether loading rate affects Fe-SMA fiber pull-out resistance.

First, Section 2 describes the pull-out failure mechanism of fibers embedded in concrete. Section 3 provides details on the materials used, the process of sample preparation, and the test methods employed in this experimental investigation. Section 4

presents the obtained results alongside a discussion and interpretation based on these results. Finally, Section 5 outlines the concluding remarks.

2. Pull-out failure mechanism

To fully comprehend the mechanism of the pull-out failure of an end-hooked fiber embedded in a concrete matrix, it is beneficial to describe the mechanism and force-displacement behavior. Figure 3 provides a schematic graph showing this mechanism. The pull-out failure of such a fiber is divided into five main stages, the first four of which are influenced by the fiber's end-hooked geometry, and the fifth stage by the surface friction between the fiber and the concrete matrix. A similar behavior and curve were observed in the current study's experiments, consistent with findings reported in previous investigations [44, 45, 46, 47].

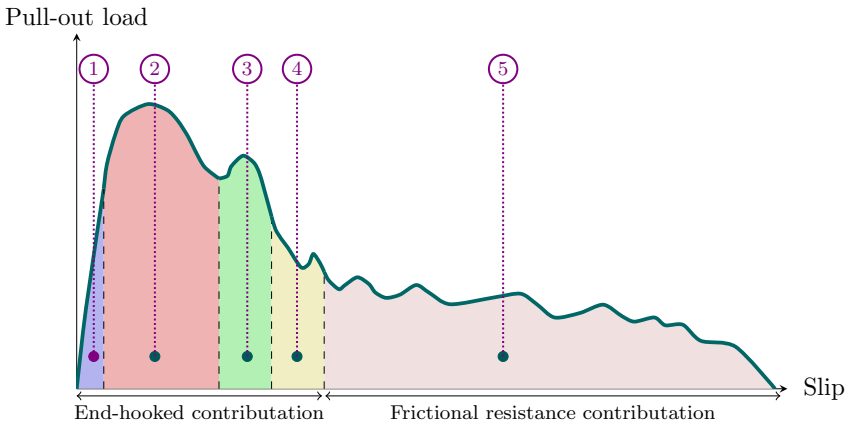

Figure 3: Schematic force-displacement behavior of the pull-out of end-hooked fiber embedded in concrete.

These stages are schematically illustrated in Figure 4 showing the pull-out failure for a single end-hooked fiber embedded in concrete.

- Stage 1: The forces are relatively low, and the behavior is linear. Unloading at this stage results in no residual displacements.
- Stage 2: As the adhesive bond loses strength, the behavior becomes non-linear and parabolic, which is due to the fiber's end-hooked form that resists the forces.

This stage and its peak force are critical for determining the fibers' pull-out resistance. A larger peak force indicates enhanced pull-out behavior. The second stage ends after the fiber's first bent shape is straightened.

- Stage 3: This stage begins when the fiber's second bent shape begins to contribute to pull-out resistance.
- Stage 4: This stage continues until the fiber's end-hooked shapes are completely straightened.
- Stage 5: At this stage, only the surface friction between the fiber and the concrete contributes to pull-out resistance. This stage continues until the fiber is completely removed from the concrete matrix and the pull-out forces drop to zero.

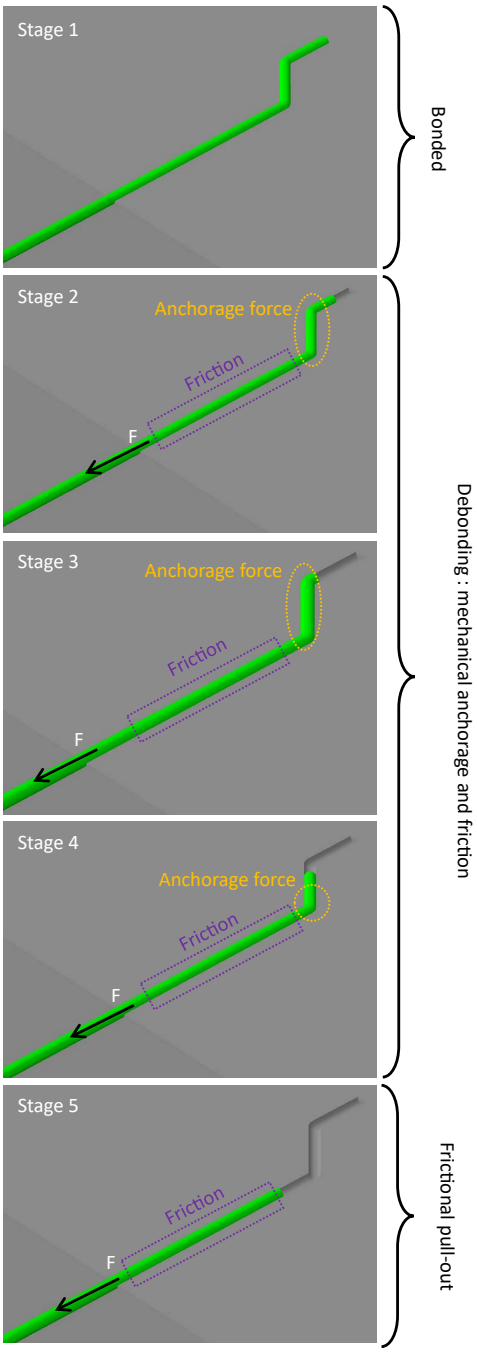

Figure 4: A schematic representation of the process of pulling out an end-hooked fiber embedded in a concrete matrix.

3. Experimental programme

This section provides a detailed presentation of the experimental methods, material properties, sample preparation, and test procedures used for measuring pull-out resistance under specified circumstances.

3.1. Materials

In the experiments, three groups of materials were used: steel rebar, concrete mix, and Fe-SMA fiber. The ribbed steel rebar had a 6 mm diameter with grade B500B steel with a specified yield strength of 500 MPa and an ultimate strain at failure of 5%.

Two different concrete mixes were designed: HPC-1 and HPC-2. The components of each mix are listed in Table 1. The main difference between these two mixes is the usage of silica fume: HPC-1 includes no silica fume, whereas HPC-2 replaces a portion of the limestone powder with an equal amount of silica fume. The mixing measures followed ASTM C192/C192M requirements [48]. Before starting on the mixer, the fine and coarse sand, some mixing water, and the admixture solution were added. Once the mixer was running, the cement and remaining water were added. After all of the components were added to the mixer, the concrete was mixed for 3 minutes, then rested for 3 minutes before being mixed for another 2 minutes. To avoid evaporation, the top of the mixer was covered during the rest. After removing the formwork following 24 hours of casting, all samples were placed in a container filled with water at a steady temperature of 20°C for 28 days before going through further tests.

Table 1: Composition of concrete mixes HPC-1 and HPC-2 (in kg/m^3).

Component	HPC-1	HPC-2
Cement II 52.5R	620	620
Limestone powder	480	360
Silica fume	0	120
Fine sand (0-0.5 mm)	301	295
Coarse sand (0.5-1.0 mm)	708	693
Superplasticizer	16.5	14.7
Shrinkage reducing agent	16.5	14.7
Water	190	190

Two types of Fe-SMA fibers were used, end-hooked and straight. Figure 5 illustrates the form and geometry of these fibers. The fibers, which were manufactured from Fe-SMA long wires with a 2.0% pre-strain level, were cut into smaller pieces before applying the end-hooked shape. Straight fibers were formed by removing the bent ends of originally end-hooked fibers. This was a result of the fiber manufacturing process and the fact that they were initially supplied for testing in an end-hooked shape.

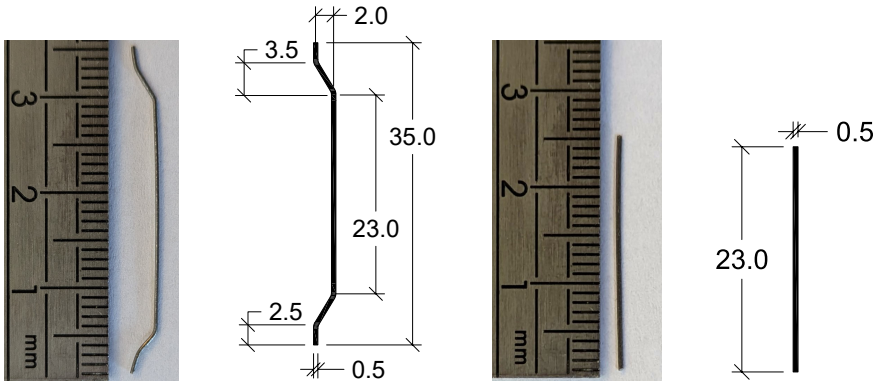

Figure 5: The geometry of (a) and (b) end-hooked, and (c) and (d) straight Fe-SMA fibers (units are in millimeters).

3.2. *Sample preparation*

Figure 6 displays the schematic of a cylindrical sample with embedded Fe-SMA fiber and steel rebar within the concrete matrix. For casting a metallic cylindrical formwork was used with 70 mm in diameter and 110 mm in height. End-hooked and straight fibers were implanted in the concrete matrix, with 17.5 mm of each fiber embedded for a consistent embedment length for both forms. This test employed a 6 mm diameter rebar with a length of 110 mm, with 55 mm embedded in the concrete matrix.

The design concept, which includes greater diameter and embedding length, as well as enhanced surface bonding (ribbed), is based on the assumption that the steel rebar remains totally anchored and has no movement, allowing for an error-free measurement of fiber pull-out resistance. Given that the rebar's embedding length is three times that of the Fe-SMA fiber, its diameter is twelve times larger, and it has a ribbed surface, it is assumed that the force applied to the Fe-SMA fiber for pull-out measurement and the reaction forces on the rebar are negligible, thus not affect the contact between the concrete matrix and steel rebar. As a result, it is believed that the steel rebar remains stationary during the test. According to Biscaia's study [49], the pull-out resistance of such rebar in concrete is typically around 20 kN, which is much greater than the pull-out resistance of Fe-SMA fiber. Furthermore, this method of determining fiber pull-out resistance is commonly used and established in the literature [50, 51, 52].

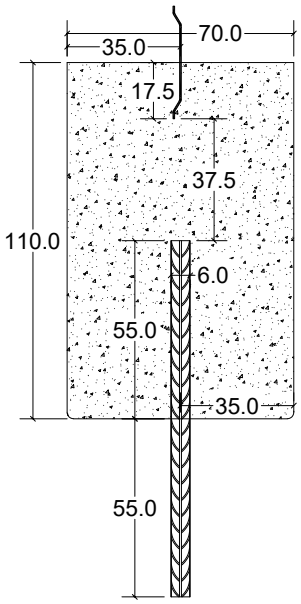

Figure 6: Schematic illustration of the cylindrical specimen used in experiments to determine the pull-out resistance of Fe-SMA fiber (units are in millimeters).

Figure 7 demonstrates the procedure used to install and fix the rebar and fiber inside the formwork and concrete matrix. Before casting, the rebar was positioned vertically on a styrofoam panel, with 55 mm of its length outside of the panel. A 6 mm diameter hole was drilled in the center of the formwork's bottom. Adhesive glue was applied around the hole and the rebar, and the formwork was placed on the rebar for a few hours to ensure proper contact and that the rebar was entirely vertical and centered. A PVC plate with a 70 mm diameter and a 0.5 mm hole in its center was used to place the Fe-SMA fiber. The adhesive held the PVC plate to the Fe-SMA fiber, ensuring that it remained in place throughout the casting. After filling the metallic formwork with fresh concrete, the PVC plate was placed on top. The small edge at the top of the formwork secured the PVC plate firmly in place, ensuring that the fiber's centerline was aligned with the steel rebar, preventing any geometrical imperfections.

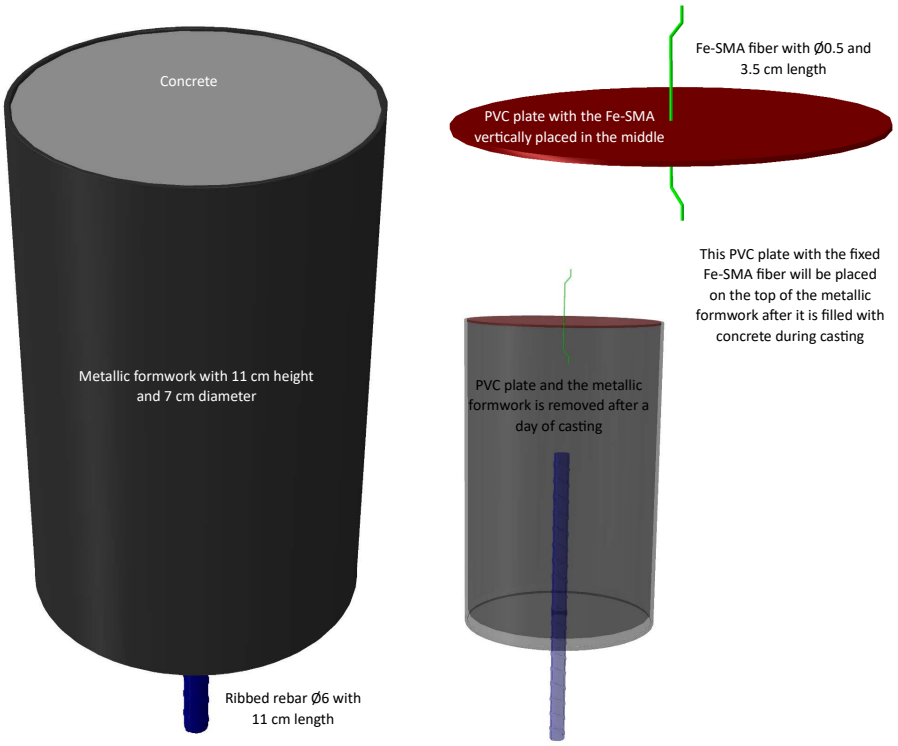

Figure 7: The procedures used to fix and install steel rebar and Fe-SMA fiber in the cylindrical formwork.

Figure 8 shows the specimen a day after casting and before removing the formwork. The PVC plate was removed, showing the fiber centered in the specimen and perpendicular to the concrete matrix's surface. The bottom view shows how the adhesive glue held the rebar centered and perpendicular to the formwork surface. Figure 9 displays pictures of the sample following the removal of the formwork and a 28-day curing period in water at 20°C. The steel rebar exhibited slight surface corrosion, which was removed before further testing to prevent slipping between the rebar and the grips.

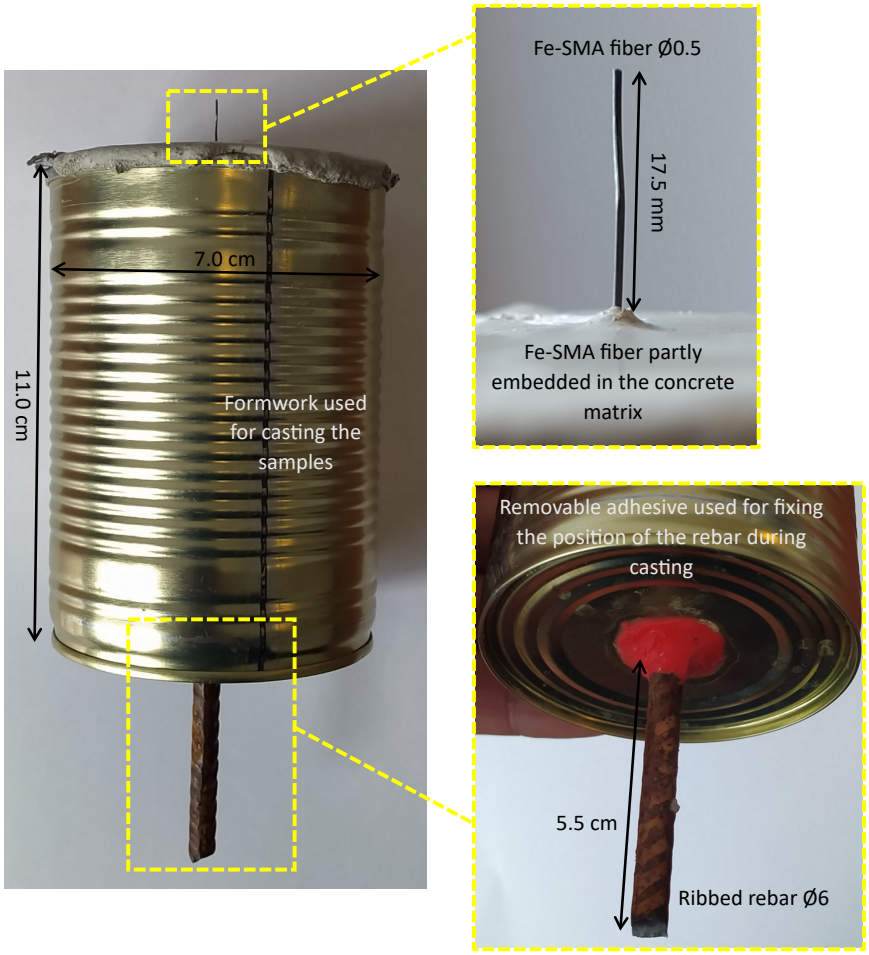

Figure 8: The cylindrical sample after casting.

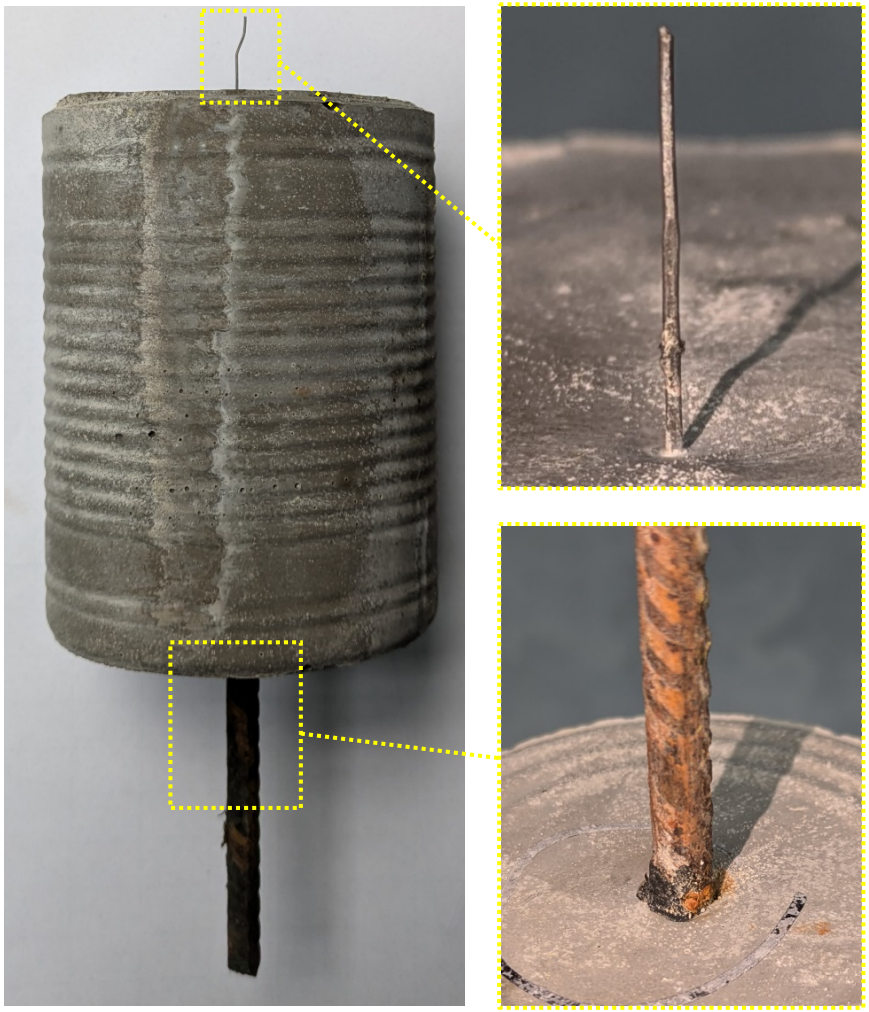

Figure 9: The cylindrical sample after removing the formwork and curing for 28 days.

In the current study, the pull-out resistance of Fe-SMA fibers was determined under various situations for comparative purposes. Two different concrete mix designs, HPC-1 and HPC-2, were used and their specifications are described before in Table 1. Two different loading rates, 0.2 mm/min and 2.0 mm/min, were used to investigate the effect of loading rate on the results. In pilot experiments, loading rates less than 2.0 mm/min were employed, although the findings were nearly identical to those at 0.2 mm/min. As a result, in the present research, the loading rate was raised 10 times to 2.0 mm/min

to identify any differences more clearly. Furthermore, two types of fibers were utilized depending on their end geometry: end-hooked and straight. Since the application of Fe-SMA fibers in concrete requires thermal activation and exposure to high temperatures, three temperature ranges were determined: ambient (no heating), 160°C, and 200°C. When thermally heated to 160°C, the Fe-SMA material exhibits recovery stresses of around 350 MPa. However, the literature indicates that increasing the temperature might partially increase recovery stress levels [53, 54, 55]. As a result, this study additionally included thermal heating at 200°C for comparative purposes.

Considering these variables, several groups of specimens were prepared and tested. Table 2 describes each type of specimen and the variable factors assigned to it. Each category was labeled depending on the variable components utilized to simplify the interpretation of the results. The minimum number of specimens was determined based on ASTM C192/C192M [48], which requires a minimum of three specimens per test. Consequently, three specimens were assigned to each of the categories identified in Table 2, and the results presented in the following sections are based on the mean outcome obtained from the three specimens in each category. A total of 72 cylindrical samples were tested for pull-out resistance using three specimens in each group, taking into account 24 different scenarios and categories.

Table 2: Specimens used for the experiments on measuring the pull-out resistance of Fe-SMA fiber.

Concrete mix	Loading rate	Fiber geometry	Temperature	Label
HPC-1	0.2 mm/min	End-hooked	Reference	HPC1-0.2-E-R
			160°C	HPC1-0.2-E-160
			200°C	HPC1-0.2-E-200
		Straight	Reference	HPC1-0.2-S-R
			160°C	HPC1-0.2-S-160
			200°C	HPC1-0.2-S-200
	2 mm/min	End-hooked	Reference	HPC1-2.0-E-R
			160°C	HPC1-2.0-E-160
			200°C	HPC1-2.0-E-200
		Straight	Reference	HPC1-2.0-S-R
			160°C	HPC1-2.0-S-160
			200°C	HPC1-2.0-S-200
HPC-2	0.2 mm/min	End-hooked	Reference	HPC2-0.2-E-R
			160°C	HPC2-0.2-E-160
			200°C	HPC2-0.2-E-200
		Straight	Reference	HPC2-0.2-S-R
			160°C	HPC2-0.2-S-160
			200°C	HPC2-0.2-S-200
	2 mm/min	End-hooked	Reference	HPC2-2.0-E-R
			160°C	HPC2-2.0-E-160
			200°C	HPC2-2.0-E-200
		Straight	Reference	HPC2-2.0-S-R
			160°C	HPC2-2.0-S-160
			200°C	HPC2-2.0-S-200

In addition to the cylindrical specimens used to measure the pull-out resistance of Fe-SMA fibers, it was essential to measure the concrete strength of each mix, as well as the effect of thermal heating on concrete strength. Following EN 1015-11 testing

standards [56], 18 beam samples (40 × 40 × 160 m^3) and 18 cube samples (40 × 40 × 40 mm^3) were prepared by cutting from beam specimens. To determine the flexural strength of the concrete, nine beam samples were prepared with the HPC-1 mix and nine with the HPC-2 mix. Similarly, nine cube samples were prepared with the HPC-1 mix and nine with the HPC-2 mix to determine the concrete's compressive strength. In each group, three samples were tested at ambient temperature, three at 160°C, and three at 200°C. To ensure uniformity in the results, the preparation, casting, and curing processes for these samples were identical to those used for cylindrical samples.

3.3. Test methods

Testing procedures include thermal heating of the specimens, measuring the flexural and compressive strength of the concrete, and measuring the pull-out resistance of Fe-SMA fiber embedded inside the concrete. The following sections provide more detail about each of these procedures.

3.3.1. Thermal heating

Thermal heating is required to trigger the phase transformation in Fe-SMA material for pre-stressing applications. Using this material in the form of short fibers randomly distributed inside a concrete matrix requires thermal heating of the entire system, including the concrete matrix. It is critical to evaluate the effect of thermal heating on the mechanical characteristics of the concrete and the pull-out resistance of Fe-SMA fibers embedded inside the matrix.

Several specimens were prepared to measure the temperature during the specimen's thermal heating. The core temperature of the samples was measured to ensure that it was uniformly distributed within the concrete matrix, allowing for a better understanding of the impact of high temperatures on concrete properties and Fe-SMA fiber pull-out resistance. Before casting these samples, a K-type thermocouple (capable of monitoring higher temperatures) was installed and fixed in each sample to guarantee the sensor was properly positioned for temperature measurements after casting. The surface temperature of the samples was also monitored to compare the external and core temperatures of the concrete. Figure 10 shows the thermocouple's position within

and outside of the cylindrical and beam specimens. During thermal heating, the thermocouple's external terminal was connected to a temperature-measuring device, which monitored the specimen's core and surface temperature. For the beam samples, the thermocouple was placed in the center of the specimen, equidistant from each side. Given the considerable difference in thermal conductivity between concrete and steel, it was assumed that the steel rebar ends located within the concrete, as well as the surrounding concrete, would heat faster than the concrete that was further from the steel rebar. For the cylindrical specimens, the thermocouple was placed 15 mm away from the rebar. This positioning ensured that the thermocouple did not make contact with the steel rebar.

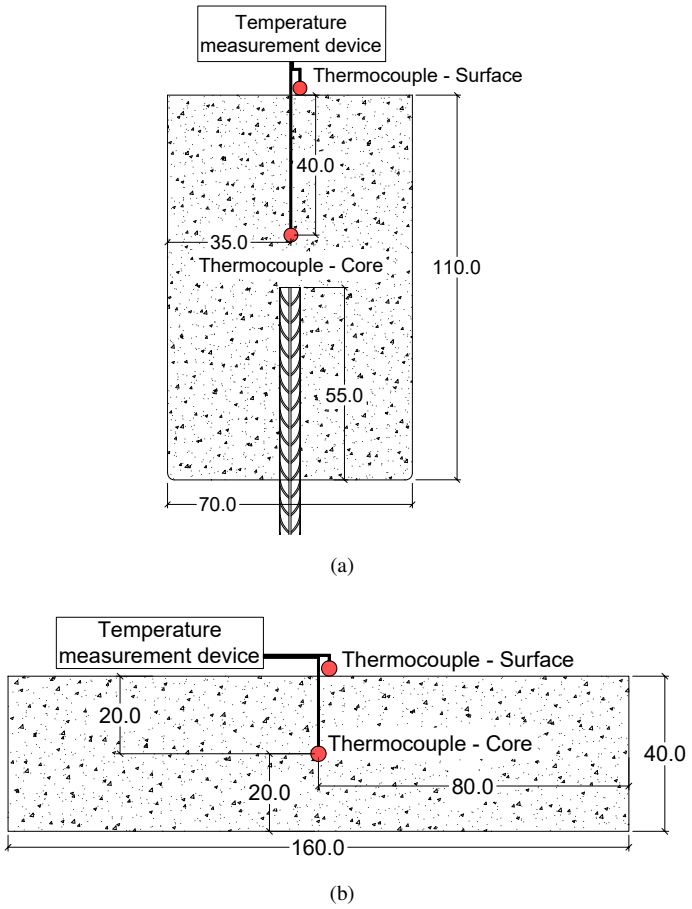

Figure 10: Schematic illustration of the thermocouple setup for temperature measurement in (a) cylindrical and (b) beam samples (units are in millimeters).

After 28 days of curing (soaked in water at 20°C), all samples were relocated to a room with an ambient temperature of 20°C and a moisture level of 40% for 12 hours to create a consistent moisture level. As seen in Figure 11, the samples selected to be heated at higher temperatures (160°C and 200°C) were put in a chamber, while the reference samples (ambient temperature) remained in the same room. The samples were placed in the middle row of the chamber, with one specimen having a thermocouple embedded in its concrete core and another thermocouple on its surface to measure the air temperature within the chamber (see Figure 12). The chamber was set to in-

crease the temperature by 8°C per minute and then maintain the target temperature once reached. Furthermore, the fans inside the chamber, placed at the top, bottom, and center, were adjusted to a rotation speed of 100 rotations per minute to improve air circulation and temperature distribution.

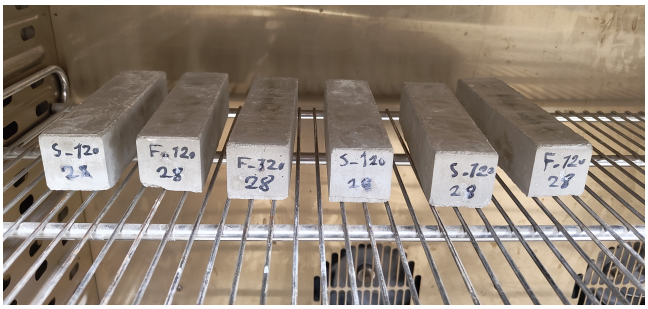

(a)

(b)

Figure 11: The specimens placed inside the chamber for thermal heating.

Figure 12: Thermocouples installed inside and on the surface of the concrete specimen to monitor the temperature during thermal heating.

3.3.2. *Flexural and compressive tests*

To determine the mechanical characteristics of each concrete mix (HPC-1 and HPC-2), as well as the impact of thermal heating on these parameters, compressive and flexural strength tests were conducted following EN 1015-11 standard [56]. As in Figure 13a, cubic specimens of 40 × 40 × 40 mm^3 were cut from beam elements and utilized for compressive testing. These cubic samples were placed in the compressing grips (40 × 40 mm^2 surface area), and displacement-controlled loading was applied at a rate of 2.0 mm per minute.

Figure 13b displays the flexural test, which employed beam samples of 40 × 40 × 160 mm^3. The samples were subjected to a three-point bending flexural test. The test consisted of a displacement-controlled grip on the top of the specimen, 80 mm from both sides (mid-span). Two rolling supports were positioned on the bottom side, 100 mm apart (30 mm from each side of the specimen). The flexural test was conducted at a loading rate of 2.0 mm per minute.

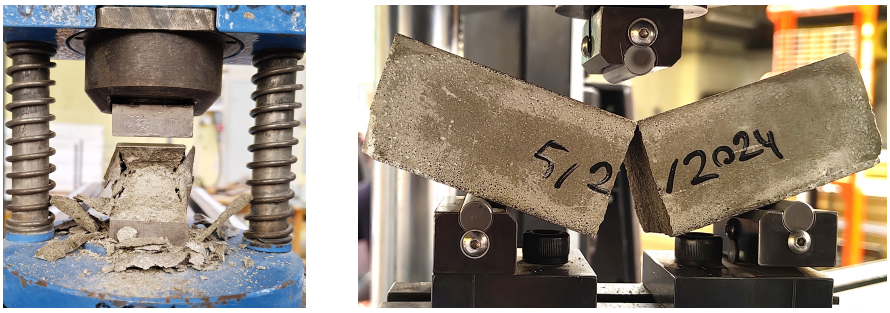

(a) (b)

Figure 13: (a) Compression test on cubic samples, (b) three-point bending test on beam samples.

3.3.3. *Pull-out test*

Figure 14 displays the test setup used for measuring the pull-out strength of Fe-SMA fiber embedded in the concrete matrix. The concrete sample, with a steel rebar embedded at the bottom and a Fe-SMA fiber on top, was placed inside the testing machine. The steel rebar was fixed in the bottom grip, which had a rounded and ribbed surface, preventing movement. The moving grip, with its flat and ribbed surface, kept

the Fe-SMA fiber in place. The grips were oriented such that the fiber and steel rebar had the same centerline, eliminating any geometrical imperfections. The moving grip applied displacement-controlled forces at rates of 0.2 and 2.0 mm/min, depending on the specimen label and its assigned loading rate. The displacement and vertical reaction forces on this grip were measured during the test.

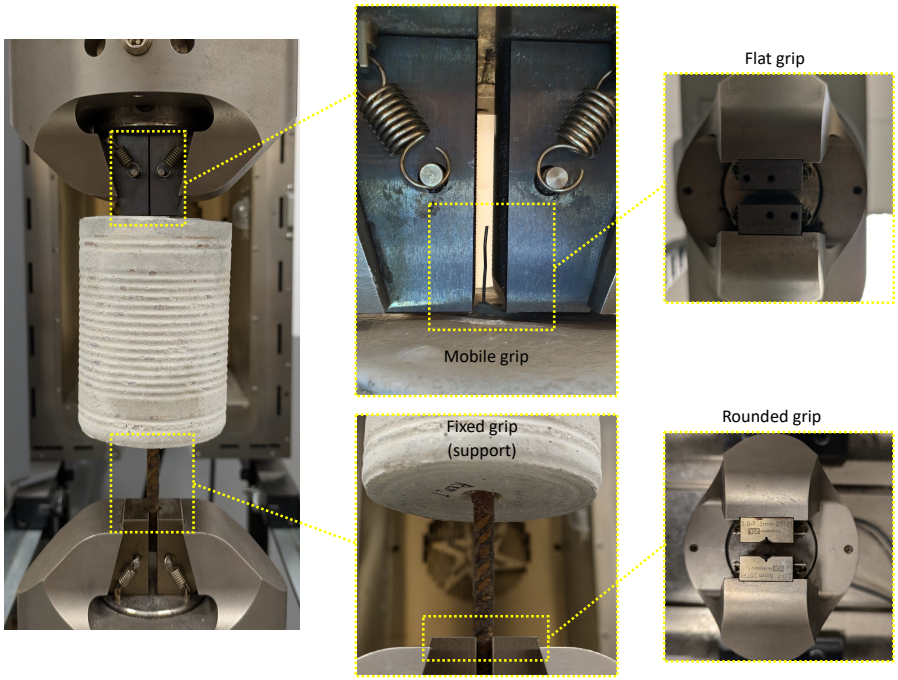

Figure 14: Test setup for the measurement of the pull-out strength of Fe-SMA fiber embedded in concrete.

4. Results and discussion

Several fibers were tested under thermal heating and mechanical loading to show the thermomechanical behavior of the Fe-SMA material used in the current study. Figure 15a shows the stress-strain curve of a Fe-SMA fiber under tensile loading (with one end fixed and the other in a mobile grip). The fiber sustained strains up to 30%, with an ultimate stress at failure of around 1150 MPa. Figure 15b shows the impact of thermal heating. The Fe-SMA fiber was fixed at both ends and exposed to a pre-load of about 100 MPa before the heating tests to avoid compression during heat-induced ex-

pansion. Within the temperature range of 24°C to 70°C, stress decreased substantially for values less than 17 MPa, which was attributable to thermal expansion. However, beyond 70°C, the stress began to grow slightly as a result of the phase transformation from martensite to austenite. As the specimen cooled, the stress increased to around 350 MPa owing to thermal contraction.

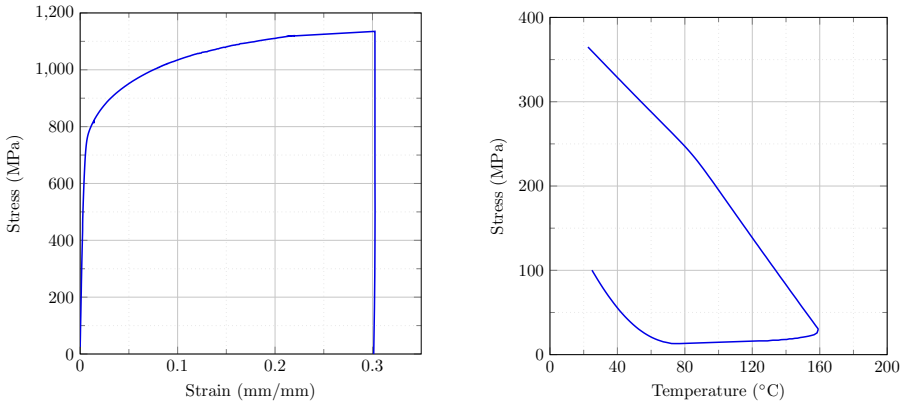

(a) (b)

Figure 15: (a) Stress-strain curve of Fe-SMA fiber under tensile loading, (b) thermal activation of pre-strained Fe-SMA fiber.

During heating, the samples' core temperatures were monitored using pre-installed thermocouples (as specified in Section 3.3.1). Figure 16 shows the measured surface and concrete core temperatures for both the beam and cylindrical samples. The beam samples required around 150 minutes to reach the temperatures of 160°C and 200°C. The cylindrical samples took around 270 minutes to reach the same temperature ranges. When the expected temperatures were reached, the chambers stopped heating and the samples were allowed to cool to ambient temperature (about 20°C). The concrete core temperature returned to room temperature after roughly 300 minutes for the beam samples and 580 minutes for the cylinder samples. Based on these results, further experiments involved heating the beam specimens for 160 minutes and the cylindrical specimens for 280 minutes. An additional 10 minutes was considered to guarantee that all specimens were heated to the required temperature, with a uniform temperature distri-

bution from the exterior surface to the core of each specimen.

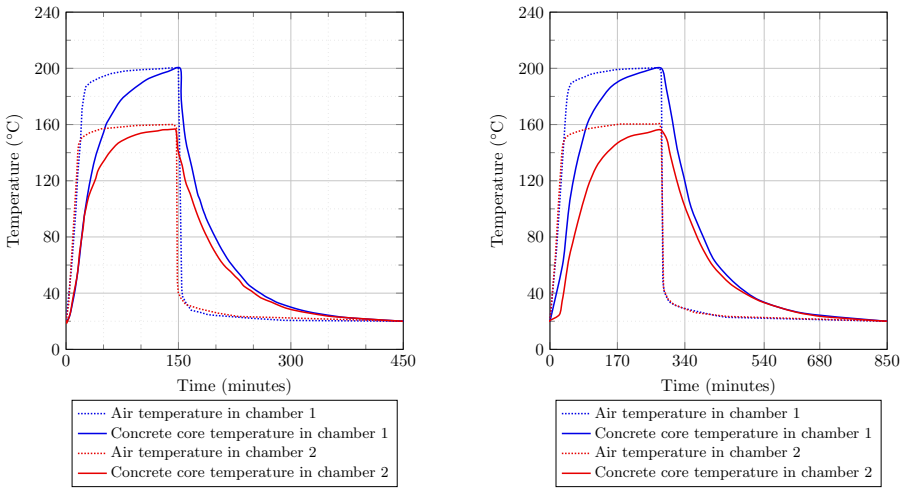

(a) Beam sample

(b) Cylindrical sample

Figure 16: The concrete's core and surface temperature measured by the installed thermocouples in (a) beam, and (b) cylindrical samples.

Before and after the thermal heating (once the samples had cooled down), their dimensions and weight were measured. Figure 17 depicts the density differences between samples of two different concrete mixes (HPC-1 and HPC-2) following exposure to thermal heating with different temperature ranges. The difference in density after heating is primarily due to water evaporation caused by high temperatures, with HPC-1 experiencing a more significant reduction in density as the temperature increases. Although HPC-1 had a slightly greater density throughout all temperature ranges, both mixes showed similar density changes when exposed to higher temperatures.

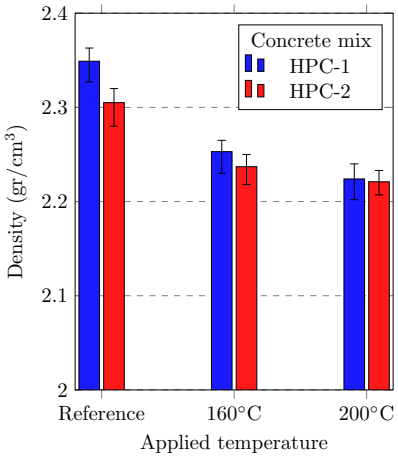

Figure 17: The effect of thermal heating on the density of different concrete mixes.

Figure 18 presents the stress-strain curves for compressive and flexural behavior of the concrete based on tests conducted on beam and cubic samples of plain concrete, with different concrete mixes and temperatures. For better comparison, Figure 19 shows the compressive and flexural strength values for each case. The sample containing HPC-1 at room temperature had the greatest compressive and flexural strengths, with 98.35 MPa and 11.5 MPa, respectively. In comparison, the HPC-2 sample had compressive and flexural strengths of 67.35 MPa and 9.72 MPa at ambient temperature. Exposing both concrete mixtures to 160°C reduced both compressive and flexural strengths. However, when exposed to 200°C, compressive and flexural strengths increased compared to 160°C, yet remained lower than the strengths of the reference samples at ambient temperature. Furthermore, the HPC-1 samples showed more significant strength changes as a result of the increase in temperature.

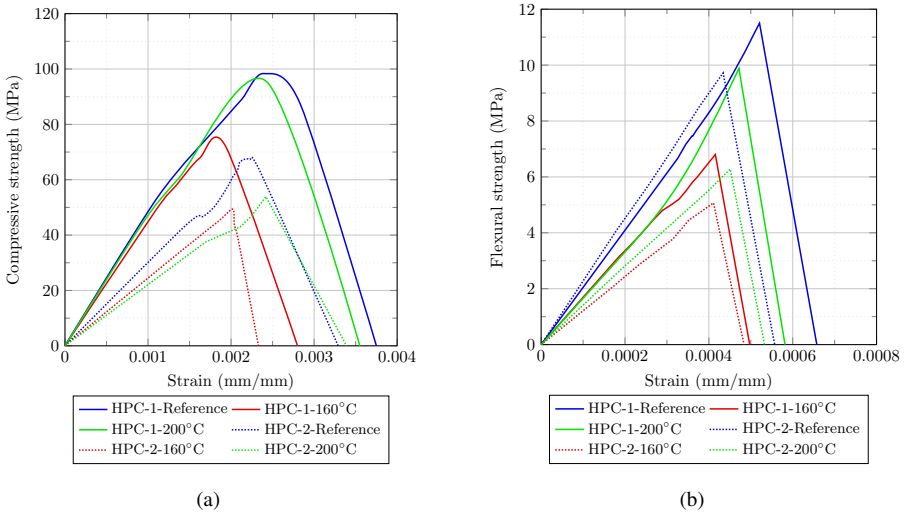

Figure 18: The effect of thermal heating on (a) compressive and (b) flexural stress-strain curves of different concrete mixes.

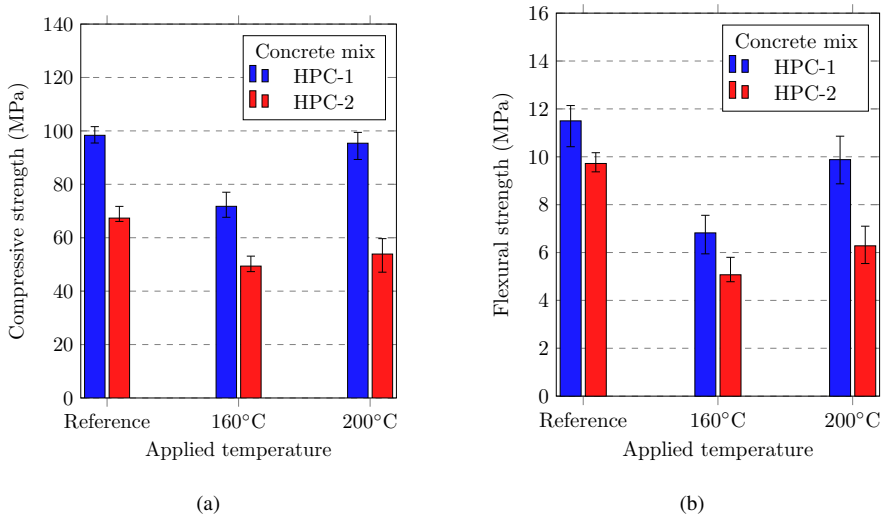

Figure 19: (a) Compressive and (b) flexural strength of different concrete mixes exposed to thermal heating at various temperature ranges.

Figure 20 shows the experimental results for the relationship between the applied

displacement at the fiber's tip, and measured pull-out force. Each curve in Figure 20 represents the average results of all specimens in each category, as described in Table 2. Figure 21 shows the maximum pull-out force for each group of specimens, with error bars indicating the range of results observed. It is important to note that for samples with end-hooked fibers, the applied displacement was limited to 16 mm. Pilot experiments revealed that frictional pull-out (Stage 5 in Figures 3 and 4) continued until the applied forces approached zero, with no substantial increase in measured forces. As a result, the testing on these samples was stopped at 16 mm of displacement, since the progression of frictional pull-out could be anticipated to end in zero force. For samples with straight fibers, the displacement was limited to 12 mm for the same reason. Furthermore, this study is primarily focused on the pull-out resistance (i.e. maximum pull-out force obtained), which occurs at the initial phase of the test. To partially observe frictional pull-out results, testing was extended to larger displacements.

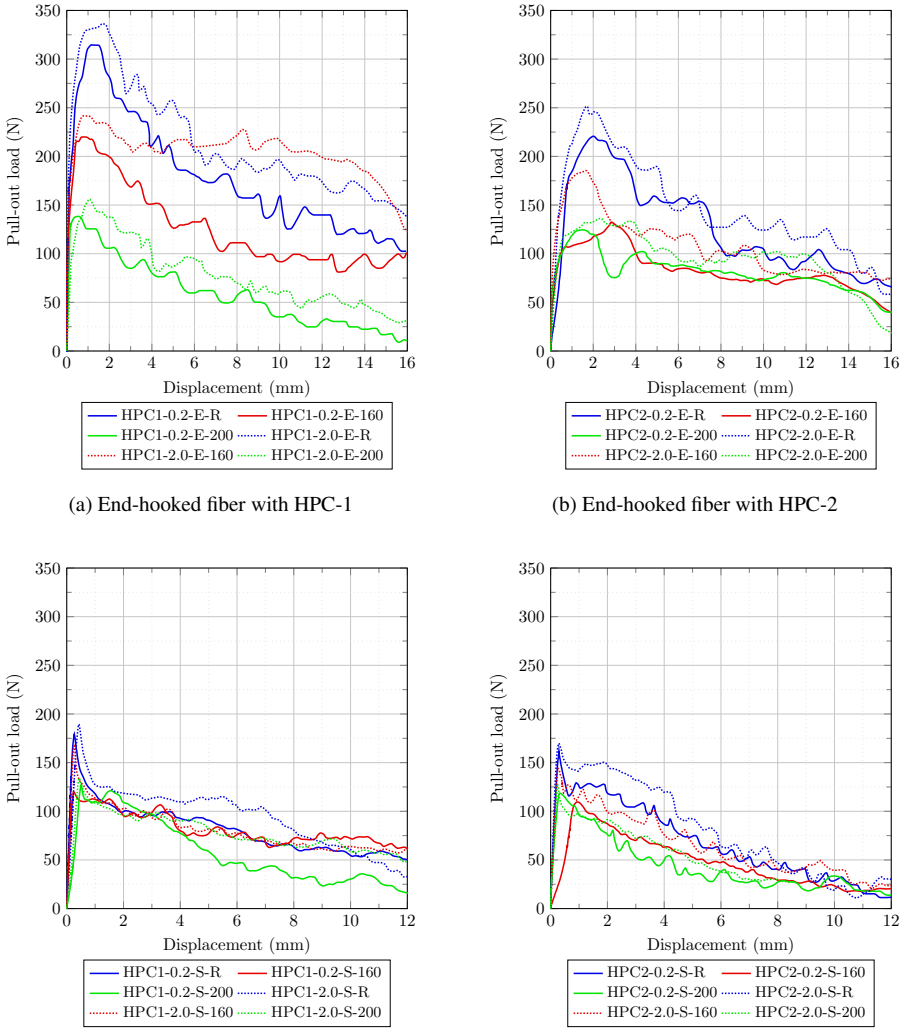

(a) End-hooked fiber with HPC-1

(b) End-hooked fiber with HPC-2

(c) Straight fiber with HPC-1

(d) Straight fiber with HPC-2

Figure 20: The average pull-out force and displacement curves for the specimens with (a) end-hooked fiber and HPC-1 mix, (b) end-hooked fiber and HPC-2 mix, (c) straight fiber and HPC-1 mix, and (d) straight fiber and HPC-2 mix.

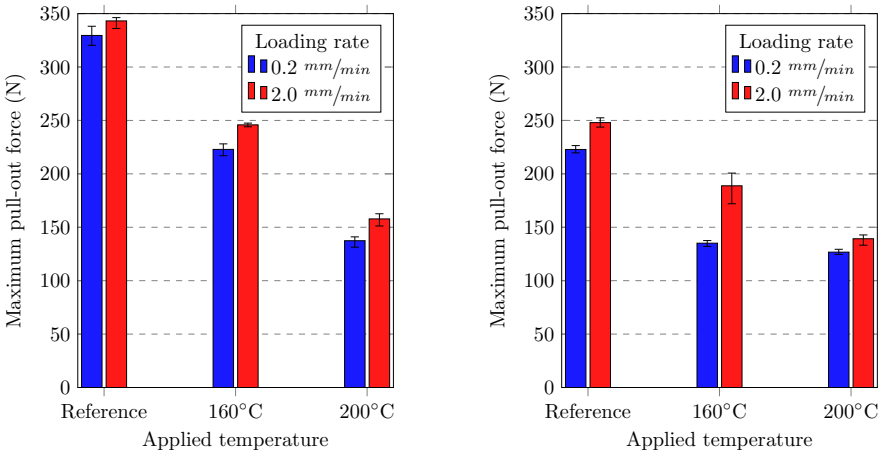

(a) End-hooked fiber with HPC-1

(b) End-hooked fiber with HPC-2

(c) Straight fiber with HPC-1

(d) Straight fiber with HPC-2

Figure 21: Pull-out resistance for the specimens with (a) end-hooked fiber and HPC-1 mix, (b) end-hooked fiber and HPC-2 mix, (c) straight fiber and HPC-1 mix, and (d) straight fiber and HPC-2 mix.

In general, the end-hooked fiber embedded in HPC-1 had the greatest pull-out resistance across all temperature and loading ratio conditions. In contrast, the straight fiber embedded in HPC-2 had the lowest pull-out resistance.

Regarding the influence of temperature on pull-out resistance, it was discovered that increasing temperature resulted in a decrease in pull-out resistance in all spec-

imens. This drop was more significant in end-hooked fibers than in straight fibers, indicating that end-hooked geometry may be less effective at higher temperatures. An exception was seen for straight fibers: whereas heating samples to 160°C greatly lowered pull-out resistance, heating to 200°C resulted in a minor increase in pull-out resistance at a moderate loading rate (0.2 mm/min), independent of concrete mix. This phenomenon requires additional investigation of the impact of loading rate and higher temperatures on the frictional pull-out resistance of Fe-SMA fibers in concrete. Furthermore, at 200°C, end-hooked fibers performed similarly to straight fibers, with only a slight increase in pull-out resistance.

Regarding loading rate, it was shown that more rapid loading rates resulted in increased pull-out resistance among all samples. Although the difference was not significant, it indicates that fibers may function better under rapid loading conditions. For the loading rate increased by ten, the change in pull-out resistance was not substantial, suggesting that this factor may be less important than geometry, temperature, and concrete mix for determining pull-out resistance. Nonetheless, the loading rate remains a significant factor in structural design.

Considering fiber shape, end-hooked fibers had higher pull-out resistance in all samples. This advantage, however, decreased as temperatures increased, independent of the concrete mix. Therefore, end-hooked fibers are suggested for applications below 200°C due to their better pull-out resistance.

In the concrete mix, fibers embedded in HPC-1 had a greater pull-out resistance, particularly end-hooked fibers. However, temperature had a greater influence on HPC-1 samples, resulting in a more substantial decrease in pull-out resistance. Despite this, HPC-1 is generally preferred because Fe-SMA fibers activated at 160°C give much better pull-out resistance when embedded in HPC-1 compared to HPC-2.

Figure 22 displays the fibers after being pulled out from the concrete matrix in two samples, which were fully removed to observe their shape post-pull-out. It can be seen that the endings of the embedded fiber have straightened, following the schematic representation in Figure 4, which represents the frictional pull-out process.

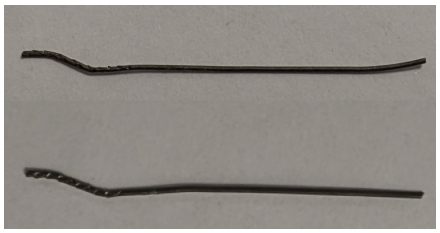

Figure 22: Fibers' shape after being pulled out from the concrete.

Figure 23 shows the concrete samples after the fibers have been completely pulled out. A comparison of samples with varying mixtures and loading rates reveals a comparable appearance at the pull-out location. However, when samples with different fiber shapes and applied temperatures are compared, differences become apparent. As a result, this figure concentrates on these two aspects. First of all, water evaporation causes the color of the concrete to change from grey to yellow, even though the photographs were taken in the same lighting and setting. End-hooked fiber samples show notable damage at the pull-out location, however, straight fibers did not result in significant damage to the concrete.

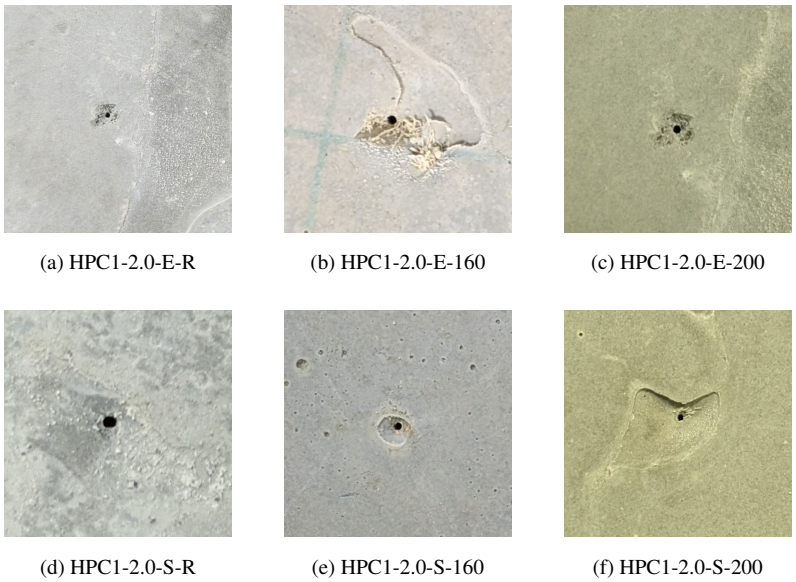

(a) HPC1-2.0-E-R (b) HPC1-2.0-E-160 (c) HPC1-2.0-E-200

(d) HPC1-2.0-S-R (e) HPC1-2.0-S-160 (f) HPC1-2.0-S-200

Figure 23: The cavity in the concrete after pulling out the Fe-SMA fiber for different samples.

To summarize, three of the four parameters tested had a substantial influence on the pull-out resistance of Fe-SMA short fibers in concrete. The loading rate has a small impact on pull-out resistance, however the fiber's end shape, concrete mix, and applied temperature have significant impacts, in that order of importance. Based on the findings, it is recommended that concrete structures with Fe-SMA fibers be carefully designed by optimizing the activation temperature, fiber end shape, and concrete mix to achieve the greatest achievable pull-out resistance.

5. Conclusions

Based on the conducted experiments and the obtained results, the following conclusions can be drawn:

- To activate the Fe-SMA fibers embedded in the concrete matrix, the entire specimen was heated to the required temperatures. It was found that exposing concrete to high temperatures might cause a loss of strength, particularly flexural strength. As a result, the design or activation method for structures with Fe-SMA short fibers should be carefully studied to minimize the detrimental impact of high temperatures on concrete strength.

- The ending shape of the Fe-SMA fibers is critical in achieving optimal pull-out resistance. End-hooked Fe-SMA fibers have been shown to give roughly double the pull-out resistance as straight fibers. Future research should look into alternative end forms, such as bent, multiple end-hooked (4D or 5D), and other alternative shapes.

- Temperature had a considerable impact on both the fiber's pull-out resistance and the concrete's strength. In general, higher temperatures reduced pull-out resistance for end-hooked fibers. However, heating the samples with straight fibers to 160°C reduced pull-out resistance, and heating to 200°C increased it when compared to the 160°C samples. Heating the concrete to 160°C decreased its compressive and flexural strength, yet heating to 200°C increased it. The

particular changes in the concrete mix between 160°C and 200°C that result in strength improvement should be studied further.

- The concrete mix had a substantial impact on the experiments. The pull-out resistance of the Fe-SMA fiber was considerably reduced in a mix with limestone powder and additional silica fume (HPC-2) compared to a mix with only limestone powder (HPC-1). Furthermore, HPC-1 had higher compressive and flexural strength at all temperatures (ambient, 160°C, and 200°C). For straight fibers, the effect of the concrete mix on pull-out resistance was insignificant, implying that friction between concrete and Fe-SMA was comparable in both mixes.
- The impact of loading rate on the pull-out resistance of Fe-SMA fibers in concrete was minimal. In summary, increasing the loading rate tenfold had a negligible effect on pull-out resistance.

Author contributions

Alireza Tabrizikahou – Conceptualization, Formal analysis, Investigation, Methodology, Project administration, Validation, Visualization, Writing – original draft. **Mieczysław Kuczma** – Resources, Supervision, Writing – review and editing. **Moslem Shahverdi** – Resources, Supervision, Writing – review and editing

Declaration of competing interest

The authors declare that they have no known competing financial interests or personal relationships that could have appeared to influence the work reported in this paper.

Data availability

Data will be made available on request.

Acknowledgements

This research was funded by the National Science Centre of Poland (Grant No. 2023/49/N/ST8/03063).

References

[1] V. Afroughsabet, L. Biolzi, T. Ozbakkaloglu, High-performance fiber-reinforced concrete: a review, Journal of Materials Science 51 (14) (2016) 6517–6551. doi:10.1007/s10853-016-9917-4.

[2] B. Li, Z. Chen, S. Wang, L. Xu, A review on the damage behavior and constitutive model of fiber reinforced concrete at ambient temperature, Construction and Building Materials 412 (2024) 134919. doi:10.1016/j.conbuildmat.2024.134919.

[3] A. A. El-Abbasy, Tensile, flexural, impact strength, and fracture properties of ultra-high-performance fiber-reinforced concrete – A comprehensive review, Construction and Building Materials 408 (2023) 133621. doi:10.1016/j.conbuildmat.2023.133621.

[4] Y. Huang, S. Grünewald, E. Schlangen, M. Luković, Strengthening of concrete structures with ultra high performance fiber reinforced concrete (UHPFRC): A critical review, Construction and Building Materials 336 (2022) 127398. doi:10.1016/j.conbuildmat.2022.127398.

[5] K. Wijesinghe, C. Gunasekara, D. W. Law, H. Hidallana-Gamage, N. Wanasekara, L. Wang, Thermal and acoustic performance in textile fibre-reinforced concrete: An analytical review, Construction and Building Materials 412 (2024) 134879. doi:10.1016/j.conbuildmat.2024.134879.

[6] M. Shahjalal, K. Islam, F. Batool, M. Tiznobaik, F. Zahid Hossain, K. Sakil Ahmed, M. S. Alam, R. Ahsan, Fiber-reinforced recycled aggregate concrete with crumb rubber: A state-of-the-art review, Construction and Building Materials 404 (2023) 133233. doi:10.1016/j.conbuildmat.2023.133233.

[7] K. Otsuka, C. M. Wayman, SShape memory materials, Cambridge University Press, Cambridge, 1998.

[8] A. Tabrizikahou, M. Kuczma, M. Łasecka-Plura, E. Noroozinejad Farsangi, M. Noori, P. Gardoni, S. Li, Application and modelling of Shape-Memory Alloys for structural vibration control: State-of-the-art review, Construction and Building Materials 342 (2022) 127975. doi:10.1016/j.conbuildmat.2022.127975.

[9] D. C. Lagoudas, Shape memory alloys: modeling and engineering applications, Springer, 2008. doi:10.1007/978-0-387-47685-8.

[10] C. Czaderski, M. Shahverdi, R. Brönnimann, C. Leinenbach, M. Motavalli, Feasibility of iron-based shape memory alloy strips for prestressed strengthening of concrete structures, Construction and Building Materials 56 (2014) 94–105. doi:10.1016/j.conbuildmat.2014.01.069.

[11] A. Cladera, B. Weber, C. Leinenbach, C. Czaderski, M. Shahverdi, M. Motavalli, Iron-based shape memory alloys for civil engineering structures: An overview, Construction and Building Materials 63 (2014) 281–293. doi:10.1016/j.conbuildmat.2014.04.032.

[12] M. Shahverdi, J. Michels, C. Czaderski, M. Motavalli, Iron-based shape memory alloy strips for strengthening RC members: Material behavior and characterization, Construction and Building Materials 173 (2018) 586–599. doi:10.1016/j.conbuildmat.2018.04.057.

[13] J. Michels, M. Shahverdi, C. Czaderski, Flexural strengthening of structural concrete with iron-based shape memory alloy strips, Structural Concrete 19 (3) (2018) 876–891. doi:10.1002/suco.201700120.

[14] S. Raza, B. Shafei, M. Saiid Saiidi, M. Motavalli, M. Shahverdi, Shape memory alloy reinforcement for strengthening and self-centering of concrete structures—State of the art, Construction and Building Materials 324 (2022) 126628. doi:10.1016/j.conbuildmat.2022.126628.

[15] A. Tabrizikahou, J. Białasik, S. Borysiak, M. Fabisiak, M. Łasecka-Plura, T. Jesionowski, M. Kuczma, Shear strengthening of damaged reinforced concrete beams with iron-based shape memory alloy (Fe-SMA) strips: numerical and parametric analysis, Archives of Civil and Mechanical Engineering 24 (3) (2024) 189. doi:10.1007/s43452-024-01004-6.

[16] A. Tabrizikahou, M. Kuczma, M. Łasecka-Plura, Out-of-Plane Behavior of Masonry Prisms Retrofitted with Shape Memory Alloy Stripes: Numerical and Parametric Analysis, Sensors 22 (20) (2022). doi:10.3390/s22208004.

[17] L. Janke, C. Czaderski, M. Motavalli, J. Ruth, Applications of shape memory alloys in civil engineering structures—Overview, limits and new ideas, Materials and Structures 38 (5) (2005) 578–592. doi:10.1007/BF02479550.

[18] B. Schranz, M. F. Nunes, C. Czaderski, M. Shahverdi, Fibre optic strain measurements for bond modelling of prestressed near-surface-mounted iron-based shape memory alloy bars, Construction and Building Materials 288 (2021) 123102. doi:10.1016/j.conbuildmat.2021.123102.

[19] M. Shahverdi, C. Czaderski, P. Annen, M. Motavalli, Strengthening of RC beams by iron-based shape memory alloy bars embedded in a shotcrete layer, Engineering Structures 117 (2016) 263–273. doi:10.1016/j.engstruct.2016.03.023.

[20] M. Shahverdi, C. Czaderski, M. Motavalli, Iron-based shape memory alloys for prestressed near-surface mounted strengthening of reinforced concrete beams, Construction and Building Materials 112 (2016) 28–38. doi:10.1016/j.conbuildmat.2016.02.174.

[21] S. Raza, J. Michels, M. Shahverdi, Uniaxial behavior of pre-stressed iron-based shape memory alloy rebars under cyclic loading reversals, Construction and Building Materials 326 (2022) 126900. doi:10.1016/j.conbuildmat.2022.126900.

[22] M. Shahverdi, S. Raza, E. Ghafoori, C. Czaderski, J. Michels, M. Motavalli, Recent Advancements in Development and Application of an Iron-based Shape Memory Alloy at Empa, CHIMIA 76 (3) (2022) 242. doi:10.2533/chimia.2022.242.

[23] C. Czaderski, M. Shahverdi, J. Michels, Iron based shape memory alloys as shear reinforcement for bridge girders, Construction and Building Materials 274 (2021) 121793. doi:10.1016/j.conbuildmat.2020.121793.

[24] K. Moser, A. Bergamini, R. Christen, C. Czaderski, Feasibility of concrete prestressed by shape memory alloy short fibers, Materials and Structures 38 (5) (2005) 593–600. doi:10.1007/BF02479551.

[25] A. Tabrizikahou, M. Kuczma, C. Czaderski, M. Shahverdi, From experimental testing to computational modeling: A review of shape memory alloy fiber-reinforced concrete composites, Composites Part B: Engineering 281 (2024) 111530. doi:10.1016/j.compositesb.2024.111530.

[26] E. Ghafoori, M. Neuenschwander, M. Shahverdi, C. Czaderski, M. Fontana, Elevated temperature behavior of an iron-based shape memory alloy used for prestressed strengthening of civil structures, Construction and Building Materials 211 (2019) 437–452. doi:10.1016/j.conbuildmat.2019.03.098.

[27] B. Schranz, J. Michels, C. Czaderski, M. Motavalli, T. Vogel, M. Shahverdi, Strengthening and prestressing of bridge decks with ribbed iron-based shape memory alloy bars, Engineering Structures 241 (2021) 112467. doi:10.1016/j.engstruct.2021.112467.

[28] S. Raza, R. Widmann, J. Michels, M. Saiid Saiidi, M. Motavalli, M. Shahverdi, Self-centering technique for existing concrete bridge columns using prestressed iron-based shape memory alloy reinforcement, Engineering Structures 294 (2023) 116799. doi:10.1016/j.engstruct.2023.116799.

[29] P. Robins, S. Austin, P. Jones, Pull-out behaviour of hooked steel fibres, Materials and Structures 35 (7) (2002) 434–442. doi:10.1007/bf02483148.

[30] G. Chanvillard, P. C. Aitcin, Pull-out behavior of corrugated steel fibers qualitative and statistical analysis, Advanced Cement Based Materials 4 (1) (1996) 28–41. doi:10.1016/1065-7355(96)00036-3.

[31] Y. M. Abbas, M. Iqbal Khan, Fiber–Matrix Interactions in Fiber-Reinforced Concrete: A Review, Arabian Journal for Science and Engineering 41 (4) (2016) 1183–1198. doi:10.1007/s13369-016-2099-1.

[32] V.-H. Ho, E. Choi, V.-M. Ngo, N.-L. Nguyen, Investigating Pullout Behavior of Inclined Superelastic SMA Fiber in a Mortar Matrix Based on Finite Element Method, Arabian Journal for Science and Engineering (apr 2024). doi:10.1007/s13369-024-09002-9.

[33] F. Isla, P. Argañaraz, B. Luccioni, Numerical modelling of steel fibers pull-out from cementitious matrixes, Construction and Building Materials 332 (2022) 127373. doi:10.1016/j.conbuildmat.2022.127373.

[34] A. Qasem, Y. S. Sallam, H. Hossam Eldien, B. H. Ahangarn, Bond-slip behavior between ultra-high-performance concrete and carbon fiber reinforced polymer bars using a pull-out test and numerical modelling, Construction and Building Materials 260 (2020) 119857. doi:10.1016/j.conbuildmat.2020.119857.

[35] Y.-S. Tai, S. El-Tawil, Computational investigation of twisted fiber pullout from ultra-high performance concrete, Construction and Building Materials 222 (2019) 229–242. doi:10.1016/j.conbuildmat.2019.06.146.

[36] L. Chen, W. Sun, B. Chen, Z. Shi, J. Lai, J. Feng, Multiscale study of fibre orientation effect on pullout and tensile behavior of steel fibre reinforced concrete, Construction and Building Materials 283 (2021) 122506. doi:10.1016/j.conbuildmat.2021.122506.

[37] J. Esmaeili, K. Andalibi, O. Gencel, F. K. Maleki, V. A. Maleki, Pull-out and bond-slip performance of steel fibers with various ends shapes embedded in polymer-modified concrete, Construction and Building Materials 271 (2021) 121531. doi:10.1016/j.conbuildmat.2020.121531.

[38] T. Soetens, A. Van Gysel, S. Matthys, L. Taerwe, A semi-analytical model to predict the pull-out behaviour of inclined hooked-end steel fibres, Construction and Building Materials 43 (2013) 253–265. doi:10.1016/j.conbuildmat.2013.01.034.

[39] A. Dehghani, F. Aslani, Y. Liu, Pullout behaviour of shape memory alloy fibres in self-compacting concrete and its relation to fibre surface microtopography in comparison to steel fibres, Construction and Building Materials 323 (2022) 126570. doi:10.1016/j.conbuildmat.2022.126570.

[40] A. Dehghani, F. Aslani, Effect of 3D, 4D, and 5D hooked-end type and loading rate on the pull-out performance of shape memory alloy fibres embedded in cementitious composites, Construction and Building Materials 273 (2021) 121742. doi:10.1016/j.conbuildmat.2020.121742.

[41] D. W. Menna, A. S. Genikomsou, M. F. Green, Effect of heat treatment and end-hook geometry on pullout behaviour of heavily cold worked superelastic NiTi shape memory alloy fibres embedded in concrete, Construction and Building Materials 361 (2022) 129630. doi:10.1016/j.conbuildmat.2022.129630.

[42] Z. Yang, Y. Du, Y. Liang, X. Ke, Mechanical Behavior of Shape Memory Alloy Fibers Embedded in Engineered Cementitious Composite Matrix under Cyclic Pullout Loads, Materials 15 (13) (2022) 4531. doi:10.3390/ma15134531.

[43] Y. Wang, F. Aslani, A. Valizadeh, An investigation into the mechanical behaviour of fibre-reinforced geopolymer concrete incorporating NiTi shape memory alloy, steel and polypropylene fibres, Construction and Building Materials 259 (2020) 119765. doi:10.1016/j.conbuildmat.2020.119765.

[44] J. Qi, Z. Wu, Z. J. Ma, J. Wang, Pullout behavior of straight and hooked-end steel fibers in UHPC matrix with various embedded angles, Construction and Building Materials 191 (2018) 764–774. doi:10.1016/j.conbuildmat.2018.10.067.

[45] F. Deng, X. Ding, Y. Chi, L. Xu, L. Wang, The pull-out behavior of straight and hooked-end steel fiber from hybrid fiber reinforced cementitious composite:

Experimental study and analytical modelling, Composite Structures 206 (2018) 693–712. doi:10.1016/j.compstruct.2018.08.066.

[46] C. Lin, T. Kanstad, S. Jacobsen, G. Ji, Bonding property between fiber and cementitious matrix: A critical review, Construction and Building Materials 378 (2023) 131169. doi:10.1016/j.conbuildmat.2023.131169.

[47] J.-H. Park, J.-H. Lee, E. Choi, C. Park, Effects of double-arched geometry and tensile strength on the pullout resistance of fibers, Case Studies in Construction Materials 19 (2023) e02316. doi:10.1016/j.cscm.2023.e02316.

[48] ASTM International, C192/C192M-19 Standard Practice for Making and Curing Concrete Test Specimens in the Laboratory (2019). doi:10.1520/C0192_C0192M-18.

[49] H. C. Biscaia, Experimental and numerical evaluations of the bond behaviour between ribbed steel rebars and concrete, Archives of Civil and Mechanical Engineering 23 (3) (2023) 159. doi:10.1007/s43452-023-00704-9.

[50] D. L. Naik, A. Sharma, R. R. Chada, R. Kiran, T. Sirotiak, Modified pullout test for indirect characterization of natural fiber and cementitious matrix interface properties, Construction and Building Materials 208 (2019) 381–393. doi:10.1016/j.conbuildmat.2019.03.021.

[51] Y. M. Abbas, Microscale Cohesive-Friction-Based Finite Element Model for the Crack Opening Mechanism of Hooked-End Steel Fiber-Reinforced Concrete, Materials 14 (3) (2021) 669. doi:10.3390/ma14030669.

[52] Y. Yao, H. Zhang, X. Zhang, F. Ren, Y. Li, Z. Yang, Experimental, Analytical and Numerical Studies of Interfacial Bonding Properties between Silane-Coated Steel Fibres and Mortar, Buildings 11 (9) (2021) 398. doi:10.3390/buildings11090398.

[53] J. Vůjtěch, P. Ryjáček, J. Campos Matos, E. Ghafoori, Iron-Based shape memory alloy for strengthening of 113-Year bridge, Engineering Structures 248 (2021) 113231. doi:10.1016/j.engstruct.2021.113231.

[54] M. Izadi, E. Ghafoori, M. Shahverdi, M. Motavalli, S. Maalek, Development of an iron-based shape memory alloy (Fe-SMA) strengthening system for steel plates, Engineering Structures 174 (2018) 433–446. doi:10.1016/j.engstruct.2018.07.073.

[55] G. Fawaz, J. Murcia-Delso, Bond behavior of iron-based shape memory alloy reinforcing bars embedded in concrete, Materials and Structures 53 (5) (2020) 114. doi:10.1617/s11527-020-01548-y.

[56] European Committee for Standardization (CEN), EN 1015–11:2020 Methods of test for mortar for masonry - Part 11: Determination of flexural and compressive strength of hardened mortar (2020).